First-principles modeling of X-ray absorption spectra enlightens the processes of scandium sequestration by iron oxides

Mathieu Chassé, Marc Blanchard, Delphine Cabaret, Amélie Juhin, Delphine Vantelon, Georges Calas

1

First-Principles Modeling of X-Ray Absorption Spectra Enlightens the Processes of Scandium Sequestration by Iron Oxides

REVISION 1

Mathieu CHASSÉ[1,*], Marc BLANCHARD[2], Delphine CABARET[1], Amélie JUHIN[1], Delphine VANTELON[3] & Georges CALAS[1]

[1]Sorbonne Université, Muséum National d'Histoire Naturelle, UMR CNRS 7590, IRD, Institut de minéralogie, de physique des matériaux et de cosmochimie, IMPMC, 75005 Paris, France

[2]Géosciences Environnement Toulouse (GET), Observatoire Midi-Pyrénées, Université de Toulouse, CNRS, IRD, UPS, 14 avenue Edouard Belin, 31400 Toulouse, France

[3]SOLEIL synchrotron, L'Orme des Merisiers, Saint-Aubin, BP 48, 91192 Gif-sur-Yvette, France

[*]Corresponding author: mathieu.chasse@normalesup.org

Abstract

Scandium is often associated with iron oxides in the environment. Despite the use of scandium as a geochemical tracer and the existence of world-class supergene deposits, uncertainties on speciation obscure the processes governing its sequestration and concentration. Here, we use first-principles approaches to interpret experimental K-edge X-ray absorption near-edge structure spectra of scandium either incorporated in or adsorbed on goethite and hematite, at concentrations relevant for the environment. This modeling helps to interpret the characteristic spectral features, providing key information to determine scandium speciation when associated with iron oxides. We show that scandium is substituted into iron oxides at low concentration without modifying the crystal structure.

2

22   When scandium is adsorbed onto iron oxide surfaces, the process occurs through outer-sphere

23   complexation with a reduction in the coordination number of the hydration shell. Considering available

24   X-ray absorption spectra from laterites, the present results confirm that scandium adsorption onto iron

25   oxides is the dominant mechanism of sequestration in these geochemical conditions. This speciation

26   explains efficient scandium recovery through mild metallurgical treatments of supergene lateritic ores.

27   The specificities of scandium sorption mechanisms are related to the preservation of adsorbed

28   scandium in million-years old laterites. These results demonstrate the emerging ability to precisely

29   model fine X-ray absorption spectral features of trace metals associated with mineral phases relevant to

30   the environment. It opens new perspectives to accurately determine trace metals speciation from high-

31   resolution spatially-resolved X-ray absorption near-edge structure spectroscopy in order to constrain

32   the molecular mechanisms controlling their dynamics.

33   **Keywords:** Scandium, XANES, Ab-Initio Calculations, Speciation, Fe oxides, Sorption, Critical Zone.

34

35   **Introduction**

36   In the critical zone (CZ: the interface between geological, hydrological and atmospheric compartments

37   where rocks interact with air, water and biota), iron oxides, in particular goethite (α–FeO(OH)) and

38   hematite (α–Fe$_2$O$_3$), are ubiquitous. They affect the biogeochemical cycling of many elements as they

39   bind through adsorption onto mineral surfaces or incorporate within the crystal structure (Brown and

40   Calas, 2012). Adsorption can also be followed by diffusive penetration into the interior of mineral

41   particles through lattice or pore diffusion (Brümmer et al. 2013). Recurring changes of the

42   biogeochemical conditions within the CZ lead to dynamic dissolution and crystallization of Fe oxides

43   controlling the fate of trace metals (e.g., Frierdich et al., 2011).

44   The fate of scandium (Sc) in the CZ is a case in point. Scandium is used as a conservative element to

45   model mass transfer during weathering (e.g., Eshel et al., 2015). The absence of accessory Sc minerals

3

46   in supergene contexts (Samson and Chassé 2016) implies that its sequestration in the CZ depends on

47   the rock-forming phases present. Scandium association with Fe oxides is well-known (Norman and

48   Haskin 1968) and illustrated by worldwide findings of Sc-rich laterites (e.g., Aiglsperger et al., 2016;

49   Chassé et al., 2017; Teitler et al., 2019), expected to become a potential source for this critical metal.

50   Nonetheless, the processes of Sc trapping in laterites remain elusive. Isomorphous substitution in Fe

51   oxides or sequestration by adsorption have been invoked in Sc-bearing laterites (Chassé et al. 2017;

52   Vind et al., 2018; Ulrich et al., 2019), making necessary an accurate determination of Sc speciation to

53   constrain Sc dynamics in the CZ.

54   In this perspective, the chemical selectivity and high sensitivity of X-ray absorption spectroscopy

55   proved to be invaluable (Chassé et al. 2017, 2019). The low Sc concentration in natural systems

56   requires the use of Sc K-edge X-ray absorption near-edge structure (XANES) spectroscopy.

57   Nonetheless, a precise analysis of Sc speciation based on XANES spectroscopy requires theoretical

58   modeling to understand the origin of the spectral features. This has been made for the first time on the

59   Sc K-edge XANES spectra of mineral compounds using first-principles calculations (Chassé et al.,

60   2018). We apply this density functional theory (DFT) approach to model XANES spectra of Sc trapped

61   by Fe oxides, stressing the interest of the method to unravel the role of incorporation and sorption

62   processes on Sc fate in the CZ.

63

64   **Experimental methods and theoretical approach**

65   We studied a Sc-chloride solution (ca. 1 wt%), Sc-substituted (ca. 1 wt%) and Sc-adsorbed (ca. 0.1 wt

66   %) goethite and hematite, and Sc-adsorbed montmorillonite ($(Na,Ca)_{0.3}(Al,Mg)_2Si_4O_{10}(OH)_2 \cdot nH_2O$,

67   ca. 1 wt%). The Sc-chloride solution was prepared by dilution of Sc^{3+} chloride hexahydrate powder.

68   Scandium-substituted goethite was prepared by maintaining a ferrihydrite suspension at 65 °C for two

69   days after precipitation from Fe^{3+} nitrate at a basic pH in presence of Sc chloride. Scandium-substituted

4

70   hematite was obtained by dehydroxylation of goethite through heating. Scandium-adsorbed samples

71   were prepared by adding a Sc-chloride solution to Sc-free synthetic goethite, hematite or natural

72   montmorillonite, later separated and dried. Details are given in Supplemental Material.

73   We recorded Sc K-edge XANES spectra at the LUCIA beamline (SOLEIL synchrotron) using an

74   Si(311) double crystal monochromator calibrated against a Sc_2O_3 standard. Measurements were

75   performed in the energy range (4400–4800) eV with energy steps of (5, 0.2, 0.5 and 1) eV in energy

76   ranges of (4400–4485) eV, (4485–4534) eV, (4534–4586) eV and (4586–4800) eV, respectively.

77   Spectra were collected at room temperature, under vacuum in XRF mode on pellets obtained from

78   powdered material and mounted on a holder between two 2 μm thick Ultralene® films, using a four-

79   element silicon drift detector (SDD). Two spectra were recorded for each reference with a counting

80   time of ca. 50 s per spectrum. The spectra acquired for each reference were merged before background

81   subtraction and normalization. Details can be found in Chassé et al. (2017).

82   Theoretical XANES spectra were calculated using the Quantum ESPRESSO plane-wave based DFT

83   suite of codes (Giannozzi et al. 2009) in the generalized gradient approximation (Perdew–Burke–

84   Ernzerhof parametrization, Perdew et al., 1996). The charge density is obtained via a relaxation of the

85   atomic positions and a self-consistent field calculation using the PWscf code. Then, XANES spectra

86   are computed in a continued fraction approach using the XSpectra code (Taillefumier et al. 2002;

87   Gougoussis et al. 2009). Computational details are given in Supplemental Material.

88   Charge density calculations were initialized using cell parameters and atomic positions obtained from

89   structure relaxations of goethite (Ducher et al. 2015) and hematite (Blanchard et al. 2008). Either one

90   or two adjacent Sc atoms (isolated or paired models, Supplemental Material) were substituted for Fe

91   atoms into the crystal structure to model Sc-substituted goethite (Fig. 1a) and hematite (Fig. 1b). It

92   corresponds to ca. 2 wt% and 4 wt% Sc for goethite models and ca. 1 wt% and 2 wt% Sc for hematite

93   models. Physiosorbed Sc was modeled by a 6-fold coordinated water complex (Rudolph and Pye

5

94   2000).

95   **Results and discussion**

96   **Spectral signature of scandium associated with iron oxides**

97   Experimental Sc K-edge XANES spectra of Sc-substituted goethite and hematite exhibit four major

98   features in the main edge (A_0, A, B and C, Fig. 2a,b), respectively located at ca. 4501 eV, 4508 eV,

99   4512 eV and 4524 eV. In the pre-edge region, two low-intensity features (P_1 and P_2), observed in

100   compounds with six-fold coordinated Sc (Lindqvist-Reis et al. 2006; Oberti et al. 2006; Chassé et al.

101   2018), are present at ca. 4492 eV and 4494 eV. The position, shape and intensity of the main-edge

102   features are reproduced in the theoretical spectra obtained from structural models of Sc-incorporated

103   goethite and hematite indicating the robustness of the calculation method and the validity of the

104   structural models (Fig. 2a,b). In the pre-edge region, the P_2 feature is less intense and split in two

105   components in the theoretical spectra (close view, Figs. 3 and S1). When Sc atoms are paired in the

106   model structure of goethite, a feature appears at higher energy (Fig. 3, *).

107   To interpret the pre-edge spectra, the DOS, correlated to the spectral features, are projected on the

108   absorbing Sc (Sc*) and its first neighbors (Fig. 3 and S1). These DOS describe, for each energy level,

109   the number of empty states available that can be reached with a certain transition probability by the

110   photoelectron during XANES experiments. The contribution of electric quadrupole (E2) transitions to

111   the P_1 and P_2 features, corresponding respectively to $1s \rightarrow 3d–t_{2g}$ and $1s \rightarrow 3d–e_g$ transitions is minor

112   (Figs. 3 and S1). Electric dipole (E1) transitions $1s \rightarrow 4p$ dominate the P features. They reflect local

113   transitions due to $4p–3d$ hybridization of Sc*, observed for non-centrosymmetric sites, such as

114   tetrahedra (Knoll et al. 2014) or distorted octahedra (Chassé et al. 2018). Non-local transitions also

115   contribute to E1 transitions and result from orbital mixing between the $4p$ orbitals of Sc* and $3d$

116   orbitals of its nearest Fe neighbors *via* the empty $2p$ orbitals of the oxygen ligands. This orbital mixing

117   of Sc* is documented for Sc-bearing compounds exhibiting $3d$ neighbors (Chassé et al. 2018). The

6

118   DOS show that the energy difference between $3d$–t_{2g} and $3d$–e_g orbitals, i.e. the crystal field splitting

119   energy (10Dq), is greater for Sc than for Fe, inducing the splitting of the P_2 feature. The 10Dq value for

120   Fe tends to be underestimated compared to experiments (Ducher et al. 2016). A higher 10Dq would

121   lead to the superimposition of the theoretical P_2 features, matching experimental spectra. When Sc

122   atoms are paired in the model structure of goethite and hematite, non-local E1 transitions may also

123   arise from orbital mixing with $3d$ orbitals of the adjacent Sc ions. Due to the absence of core hole on

124   these neighbors, the position of the $3d$ orbitals is at higher energies, leading to additional features on

125   the calculated pre-edge (Figs. 3 and S1, shown as *, at ca. 4497 eV for goethite and at ca. 4496 eV and

126   4498 eV for hematite), absent from experimental spectra. This additional feature is unambiguous in the

127   hematite spectrum when plotting the different polarization dependent components of the isotropic

128   spectrum (Fig. S2). Such additional pre-edge features are also observed for Sc oxides (Chassé et al.

129   2018) and for other $3d$ ions in oxides such as Ti^{4+} (Cabaret et al. 2010) and Cr^{3+} ions (Verger et al.

130   2016) accounting for the presence of neighbors with the same nature as the absorbing atom.

131

132   **Atomic environment of scandium associated to iron oxides**

133   The agreement between experimental and theoretical spectra in the main edge confirms the structural

134   incorporation of Sc in the synthesized Fe oxides. Despite small discrepancies in the energy and

135   intensity of some transitions, inherent to the limitation of DFT-based methods to model the core–hole

136   electron interaction and the $3d$ electron–electron repulsion (Cabaret et al. 2010), the transitions

137   observed in the pre-edge are reproduced and interpreted from the projected DOS. The absence of the

138   feature diagnostic of Sc pairing (Figs. 3 and S1, *) in experimental spectra of goethite and hematite

139   indicates that substituted Sc sites are isolated. A correct modeling of the spectra does not require

140   volume-cell relaxation. At low Sc concentrations, below a few wt%, the structure of these Fe oxides

141   accommodates Sc substitution without significant changes in the cell volume, the changes in Sc–O

7

142   distances relative to Fe–O distances remaining low (< 7 %, Supplemental Table S1). When Sc is

143   structurally incorporated, it is dispersed at low concentration, without modifying the Fe-oxides cell

144   volume.

145   Scandium K-edge XANES spectra of Sc-adsorbed goethite and hematite are similar and alike that of Sc

146   adsorbed on Fe-free clay surfaces (Fig. 2c). Specific affinity for a given site of Fe-oxide surfaces and

147   adsorption through covalent bonding is thus excluded. Scandium binding must occur through outer

148   sphere complexes. Comparison with such Sc complexes indicates that the splitting of the pre-edge

149   associated with the low intensity of the main edge is consistent with six-fold coordinated complexes

150   but incompatible with higher coordination numbers (Fig. 2c, Sc-chloride solution and Lindqvist-Reis et

151   al., 2006; Yamaguchi et al., 1997). A theoretical spectrum is calculated using an isolated 6-fold

152   coordinated $[Sc(H_2O)_4(OH)_2]^+$ complex, $Sc(OH)_2^+$ being the dominant species at the slightly acidic pH

153   of adsorption experiments (Wood and Samson 2006). The calculated spectrum reproduces the major

154   features exhibited by experimental spectra (A and B, Fig. 2c). The splitting of the pre-edge and the

155   relative intensity of the two features is reproduced (P_1 and P_2, Fig. 2c). Despite discrepancies in this

156   region arising from the simpleness of the model, the closeness between the calculated spectrum and the

157   experimental spectra of adsorbed Sc indicates that adsorption results in a reduction of the coordination

158   number of the Sc^{3+} complex. This complex is seven- to nine-fold coordinated in solution

159   (Vchirawongkwin et al. 2012, illustrated by the spectrum of the Sc-chloride solution, Fig. 2c) and six-

160   fold coordinated at the surface of Fe oxides (illustrated by the spectrum of Sc-adsorbed goethite and

161   hematite, Fig. 2c). The lability of the Sc^{3+} hydration shell supports this observation (Migliorati and

162   D'Angelo 2016).

163

164   **Mechanisms of scandium sequestration by iron oxides in the critical zone**

165   First-principles calculations do not show significant difference of affinity for Sc substitution in goethite

8

166   or hematite (ΔE_{Gt-Hem} = 0.33 eV, Supplemental Material and Table S2). Preferential incorporation into

167   goethite (Ulrich et al. 2019) or hematite (Vind et al., 2018) must reflect the role of the conditions of

168   formation in determining the nature of the phase incorporating Sc, as shown for lutetium (Yokosawa et

169   al. 2019). In particular, differences in specific surface area or distinct precursor phases during Fe oxides

170   crystallization can explain variations in affinity for Sc. Sorption to goethite in lateritic Fe oxide-rich

171   horizons plays a major role in Sc trapping and concentration processes (Chassé et al. 2019). The

172   theoretical modeling of the spectra of outer-sphere Sc complexes exhibit features for which the

173   position, intensity and shape are comparable to experimental spectra of Sc-adsorbed species and bulk

174   lateritic samples (Fig. 2c). The agreement with experimental spectra of Sc-substituted goethite and

175   hematite excludes trapping by structural incorporation within crystallized Fe oxides in supergene

176   contexts, despite the existence of a solid solution $Fe_xSc_{(1-x)}O(OH)$ in mild hydrothermal conditions (70

177   °C, Levard et al., 2018). Subtle differences between spectra of lateritic samples and Sc-adsorbed Fe

178   oxides (Fig. 2c, +), close to major features observed in Sc-substituted reference spectra, indicate minor

179   incorporation. With aging, as other metallic ions (Brümmer et al., 2013), Sc could penetrate Fe oxides

180   following adsorption processes enhanced by nanoporosity or lattice diffusion. The physico-chemical

181   parameters and growth kinetics are key determinants of the mechanism of Sc sorption. At increasing

182   metal concentration in solution, the process of adsorption through complexation at goethite surface may

183   be replaced by the formation of surface precipitates and structural incorporation, such as is the case for

184   nickel (Ugwu et al. 2019). At environmental conditions, with low Sc concentrations (< a few tenth

185   of wt%) and room temperature (ca. 30 °C on average under tropical climates), the surface complexation

186   process and slow kinetics must favor Sc adsorption onto goethite at the expense of structural

187   incorporation. In particular, the kinetics of this process in competition with successive dissolution and

188   crystallization processes may lead to the preservation of Sc complexes during the formation and

189   evolution of lateritic profiles.

9

190

Implications

191

192 **A speciation explaining mineral processing results.** The speciation of critical metals has direct

193 implications for ore processing. For instance, cobalt sorption to goethite is mainly irreversible when

194 forming monodentate complexes while leaching remains efficient when polydentate polynuclear

195 complexes form (Ugwu and Sherman, 2017). The preservation of Sc sorbed onto Fe oxides surfaces in

196 laterites explains why Sc is efficiently recovered from lateritic ores using ion exchange (79 % recovery,

197 Williams-Jones and Vasyukova, 2018) or high-pressure acid leaching processes (94 % recovery with

198 limited Fe-oxides dissolution, Wang et al., 2011).

199 **An original sorption process controlling Sc fate in the critical zone.** The nature of the adsorption

200 process may be of importance to the stability of Sc sorption after aging. The exchange of water

201 molecules inside the solvation shell of Sc with the solvent is eased by the existence of a far-coordinated

202 water molecule capping the complex (Migliorati and D'Angelo 2016), facilitating geometric changes

203 required for Sc adsorption and stabilizing the six-fold coordinated complex. The persistence of

204 adsorbed Sc species in million-years old laterites may result from this original sorption mechanism.

205 **A promising tool to study the speciation of trace metals in the critical zone.** This study

206 demonstrates that state-of-the-art first-principles calculations can reproduce XANES spectra of metals

207 associated with phases ubiquitous in the CZ. The complexity of the pathways leading to Sc trapping in

208 the CZ and their dependence to varying environmental conditions are evidenced. As for other trace

209 metals, experimental sequestration on model systems prepared in diverse but controlled conditions are

210 required as references to determine speciation in natural contexts. This theoretical tool, combined to

211 XANES, offers a new opportunity to make the link between experiments and natural environments to

212 obtain direct information on the molecular environment of trapping at trace concentration.

213 **Future directions for first-principles-assisted investigation in environmental mineralogy.** X-ray

214 absorption spectroscopy has become a central tool in environmental sciences (Brown and Calas 2012).

215 In the case of transition elements, the pre-edge features are used to determine element speciation but

216 their understanding is still complicated by the limitation of DFT-based approaches in this region. A

217 better modeling of the core-hole effects and of electron-electron interactions in DFT-based software is

218 developed (e.g., Cabaret et al. 2010) and will further improve the agreement between experimental and

219 calculated pre-edge spectra. Another direction, specific to adsorbed elements, would be to combine

220 DFT-based calculations of X-ray absorption spectra with DFT-based molecular dynamic simulations to

221 determine the molecular environments of adsorption and their energies (e.g., Watts et al. 2019).

222

Acknowledgements

228

References

230 Aiglsperger, T., Proenza, J.A., Lewis, J.F., Labrador, M., Svojtka, M., Rojas-Purón, A., Longo, F. and
231 Durišová, J. (2016) Critical metals (REE, Sc, PGE) in Ni laterites from Cuba and the Dominican
232 Republic. Ore Geology Reviews, 73, 127–147.

233 Blanchard, M., Lazzeri, M., Mauri, F. and Balan, É. (2008) First-Principles Calculation of the Infrared
234 Spectrum of Hematite. American Mineralogist, 93, 1019–1027.

235 Brown Jr. G.E. and Calas G. (2012) Mineral–Aqueous Solution Interfaces and Their Impact on the
236 Environment. Geochemical Perspectives, 1, 483–742.

237 Brümmer, G.W., Barrow, N.J. and Fischer, L. (2013) Effect of Porosity of Goethite on the Sorption of
238 Six Heavy Metal Ions: Sorption of Metals by Different Goethites. European Journal of Soil Science,

11

239   64, 805–813.

240   Cabaret, D., Bordage, A., Juhin, A., Arfaoui, M., and Gaudry, E. (2010) First-Principles Calculations of
241   X-Ray Absorption Spectra at the *K*-Edge of 3*d* Transition Metals: an Electronic Structure Analysis of
242   the Pre-Edge. Physical Chemistry Chemical Physics, 12, 5619–5633.

243   Chassé, M., Griffin, W.L., O'Reilly, S.Y. and Calas, G. (2017) Scandium Speciation in a World-Class
244   Lateritic Deposit. Geochemical Perspectives Letters, 3, 105-114.

245   Chassé, M., Juhin, A., Cabaret, D., Delhommaye, S., Vantelon, D. and Calas, G. (2018) Influence of
246   Crystallographic Environment on Scandium *K*-Edge X-Ray Absorption Near-Edge Structure Spectra.
247   Physical Chemistry Chemical Physics, 20, 23903.

248   Chassé, M., Griffin, W.L., O'Reilly, S.Y. and Calas, G. (2019) Australian Laterites Reveal Mechanisms
249   Governing Scandium Dynamics in the Critical Zone. Geochimica Cosmochimica Acta, 260, 292–310.

250   Ducher, M., Blanchard, M., Vantelon, D., Nemausat, R. and Cabaret, D. (2016) Probing the Local
251   Environment of Substitutional Al^{3+} in Goethite Using X-Ray Absorption Spectroscopy and First-
252   Principles Calculations. Physics and Chemistry of Minerals, 43, 1-11.

253   Eshel, G., Lin, C. and Banin, A. (2015) Novel Approach for Quantitatively Estimating Element
254   Retention and Material Balances in Soil Profiles of Recharge Basins Used for Wastewater Reclamation.
255   Science of the Total Environment, 502, 517-525.

256   Frierdich, A.J., Luo, Y. and Catalano, J.G. (2011) Trace Element Cycling Through Iron Oxide Minerals
257   During Redox-Driven Dynamic Recrystallization. Geology, 39, 1083–1086.

258   Giannozzi, P., Baroni, S., Bonini, N., Calandra, M., Car, R., Cavazzoni, C., Ceresoli, D., Chiarotti,
259   G.L., Cococcioni, M., Dabo, I., Dal Corso, A., De Gironcoli, S., Fabris, S., Fratesi, G., Gebauer, R.,
260   Gerstmann, U., Gougoussis, C., Kokalj, A., Lazzeri, M., Martin-Samos, L., Marzari, N., Mauri, F.,
261   Mazzarello, R., Paolini, S., Pasquarello, A., Paulatto, L., Sbraccia, C., Scandolo, S., Sclauzero, G.,
262   Seitsonen, A.P., Smogunov, A., Umari, P. and Wentzcovitch, R.M. (2009) QUANTUM ESPRESSO: A
263   Modular and Open-Source Software Project for Quantum Simulations of Materials. Journal of Physics:
264   Condensed Matter, 21, 395502.

265   Gougoussis, C., Calandra, M., Seitsonen, A.P. and Mauri, F. (2009) First-Principles Calculations of X-
266   Ray Absorption in a Scheme Based on Ultrasoft Pseudopotentials: From α-Quartz to High-T_c
267   Compounds. Physical Review B, 80, 1-8.

268   Knoll, S.M., Rovezzi, M., Zhang, S., Joyce, T.B., and Moram, M.A. (2014) Electronic Structure and
269   Local Distortions in Epitaxial ScGaN Films. Journal of Physics: Condensed Matter, 26, 225801.

270   Levard, C., Borschneck, D., Grauby, O., Rose, J. and Ambrosi, J.-P. (2018) Goethite, a Tailor-Made
271   Host for the Critical Metal Scandium: The $Fe_xSc_{(1-x)}OOH$ solid solution. Geochemical Perspectives

12

272   Letters, 9, 16-20.

273   Lindqvist-Reis, P., Persson, I. and Sandström, M. (2006) The Hydration of the Scandium(III) Ion in
274   Aqueous Solution and Crystalline Hydrates Studied by XAFS Spectroscopy, Large-Angle X-Ray
275   Scattering and Crystallography. Dalton Transactions, 32, 3868-3878.

276   Migliorati, V. and D'Angelo, P. (2016) Unraveling the Sc^{3+} Hydration Geometry: The Strange Case of
277   the Far-Coordinated Water Molecule. Inorganic Chemistry, 55, 6703-6711.

278   Norman, J.C. and Haskin, L.A. (1968) The Geochemistry of Sc: A Comparison to the Rare Earths and
279   Fe. Geochimica Cosmochimica Acta, 32, 93–108.

280   Oberti, R., Quartieri, S., Dalconi, M.C., Boscherini, F., Iezzi, G., Boiocchi, M., and Eeckhout, S.G.
281   (2006) Site Preference and Local Geometry of Sc in Garnets: Part I. Multifarious Mechanisms in the
282   Pyrope--Grossular Join. American Mineralogist, 91, 1230–1239.

283   Perdew, J. P., Burke, K. and Ernzerhof, M. (1996) Generalized Gradient Approximation Made Simple.
284   Physical Review Letters, 77, 3865-3868.

285   Rudolph, W.W. and Pye, C.C. (2000) Raman Spectroscopic Measurements of Scandium(III) Hydration
286   in Aqueous Perchlorate Solution and Ab Initio Molecular Orbital Studies of Scandium(III) Water
287   Clusters: Does Sc(III) Occur as a Hexaaqua Complex? The Journal of Physical Chemistry A, 104,
288   1627-1639.

289   Samson, I.M. and Chassé, M. (2016) Scandium. In W.M. White, Ed., Encyclopedia of Geochemistry, p.
290   1-5. Springer International Publishing, Cham.

291   Taillefumier, M., Cabaret, D., Flank, A.-M. and Mauri, F. (2002) X-ray Absorption Near-Edge
292   Structure Calculations with the Pseudopotentials: Application to the *K*-edge in Diamond and α-Quartz.
293   Physical Review B, 66, 195107.

294   Teitler, Y., Cathelineau, M., Ulrich, M., Ambrosi, J.-P., Muñoz, M. and Sevin, B. (2019) Petrology and
295   Geochemistry of Scandium in New Caledonian Ni-Co Laterites. Journal of Geochemical Exploration,
296   196, 131-155.

297   Ugwu, I.M. and Sherman, D.M. (2017) Irreversibility of Sorption of Cobalt to Goethite (α-FeOOH)
298   and Disparities in Dissolution of Aged Synthetic Co-Goethite. Chemical Geology, 467, 168–176.

299   Ugwu, I.M., Sherman, D.M. and Bacon, C.G.D. (2019) Sorption of Nickel Onto Goethite (α-FeOOH)
300   and Desorption Kinetics of Aged Synthetic Ni-Goethite: Implication for Ni Laterite Ore. Chemical
301   Geology, 509, 223–233.

302   Ulrich, M., Cathelineau, M., Muñoz, M., Boiron, M.-C., Teitler, Y. and Karpoff, A.-M. (2019) The
303   Relative Distribution of Critical (Sc, REE) and Transition Metals (Ni, Co, Cr, Mn, V) in Some Ni-
304   Laterite Deposits of New Caledonia. Journal of Geochemical Exploration, 197, 93-113.

13

305 Vchirawongkwin, V., Kritayakornupong, C., Tongraar, A. and Rode, B.M. (2012) Characterization of
306 Structure and Dynamics of an Aqueous Scandium(III) Ion by an Extended Ab Initio QM/MM
307 Molecular Dynamics Simulation. Dalton Transactions, 41, 11889.

308 Verger, L., Dargaud, O., Rousse, G., Rozsályi, E., Juhin, A., Cabaret, D., Cotte, M., Glatzel, P., and
309 Cormier, L. (2016) Spectroscopic properties of Cr^{3+} in the spinel solid solution $ZnAl_{2-x}Cr_xO_4$. Physics
310 and Chemistry of Minerals, 43, 33–42.

311 Vind, J., Malfliet, A., Bonomi, C., Paiste, P., Sajó, I.E., Blanpain, B., Tkaczyk, A.H., Vassiliadou, V.
312 and Panias, D. (2018) Modes of Occurrences of Scandium in Greek Bauxite and Bauxite Residue.
313 Mineral Engineering, 123, 35-48.

314 Wang, W., Pranolo, Y. and Cheng, C.Y. (2011) Metallurgical Processes for Scandium Recovery from
315 Various Resources: a Review. Hydrometallurgy, 108, 100-108.

316 Watts, H.D., O'Day, P.A., and Kubicki, J.D. (2019) Gibbsite (100) and Kaolinite (100) Sorption of
317 Cadmium(II): A Density Functional Theory and XANES Study of Structures and Energies. The Journal
318 of Physical Chemistry A, 123, 6319–6333.

319 Williams-Jones, A.E. and Vasyukova, O.V. (2018) The Economic Geology of Scandium, the Runt of
320 the Rare Earth Element Litter. Economic Geology, 113, 973-988.

321 Wood, S.A. and Samson, I.M. (2006) The Aqueous Geochemistry of Gallium, Germanium, Indium and
322 Scandium. Ore Geology Reviews, 28, 57-102.

323 Yamaguchi, T., Niihara, M., Takamuku, T., Wakita, H. and Kanno, H. (1997) Scandium(III) hydration
324 in aqueous solution from X-ray diffraction and X-ray absorption fine structure measurements.
325 Chemical Physics Letters, 274, 485–490.

326 Yokosawa, T., Prestat, E., Polly, R., Bouby, M., Dardenne, K., Finck, N., Haigh, S.J., Denecke, M.A.
327 and Geckeis, H. (2019) Fate of Lu(III) Sorbed on 2-Line Ferrihydrite at pH 5.7 and Aged for 12 Years
328 at Room Temperature. II: Insights from STEM-EDXS and DFT Calculations. Environmental Science
329 and Pollution Research, 26, 5282-5293.

330

331

332

333

334

335

336

14

337

338

339 **List of figures**

340 **Figure 1** Representations of the supercells of Sc-substituted goethite (2 × 1 × 3) **(a)** and hematite

341 (2 × 2 × 1) **(b)**, and of the $[Sc(H_2O)_4(OH)_2]^+$ model complex **(c)** considered in the present study. The

342 two-tone sites can either be occupied by Fe (isolated model) or by Sc (paired model).

343 **Figure 2** Comparison between experimental (red) and calculated (black) normalized Sc K-edge

344 XANES spectra for Sc-substituted goethite **(a)** and hematite **(b)** and Sc-adsorbed goethite and hematite

345 **(c)**. Additional reference spectra of a $ScCl_3$ solution (ca. 1 wt% Sc), Sc-adsorbed montmorillonite

346 (ca. 1 wt% Sc) and from a lateritic sample (ca. 750 ppm Sc, Chassé et al. 2017) are given for

347 comparison in **(c)**. Calculated spectra are shifted in energy to match the experimental A feature. The

348 symbols + indicate features discussed in the paper.

349 **Figure 3** Experimental and calculated pre-edge regions of Sc K-edge XANES spectra of Sc-substituted

350 goethite: **(a)** isolated structural model; **(b)** paired structural model. The calculated electric dipole (E1)

351 and quadrupole (E2) contributions are displayed. The partial densities of the absorbing Sc (Sc*) $4p$ and

352 $3d$ states, of the first six O neighbors $2p$ states, of the first Fe and Sc neighbors $3d$ states are shown.

353 The energy scale of the experimental spectra is shifted to match calculated spectra. The vertical line

354 indicates the Fermi level (E_F). The * symbol indicate features discussed in the paper.

Feuille1

	Goethite		
	Interatomic distances (Å)		
Oxygen neighbor	Fe–O	Sc–O (isolated)	Difference relative to Fe–O distances (%)
O1	1.90	2.03	6.84
O2	1.98	2.07	4.55
O3	1.98	2.07	4.55
O4	2.12	2.16	1.89
O5	2.12	2.16	1.89
O6	2.14	2.15	0.47
	Hematite		
	Interatomic distances (Å)		
Oxygen neighbor	Fe–O	Sc–O (isolated)	Difference relative to Fe–O distances (%)
O1	1.93	2.04	5.70
O2	1.93	2.04	5.70
O3	1.93	2.04	5.70
O4	2.14	2.17	1.40
O5	2.14	2.17	1.40
O6	2.14	2.17	1.40

Table S1

Feuille1

Sc–O (paired)	Difference relative to Fe–O distances (%)
2.03	6.40
2.04	2.94
2.08	4.81
2.16	1.85
2.16	1.85
2.15	0.47

Sc–O (paired)	Difference relative to Fe–O distances (%)
2.03	5.18
2.03	5.18
2.03	5.18
2.19	2.34
2.19	2.34
2.19	2.34

Feuille1

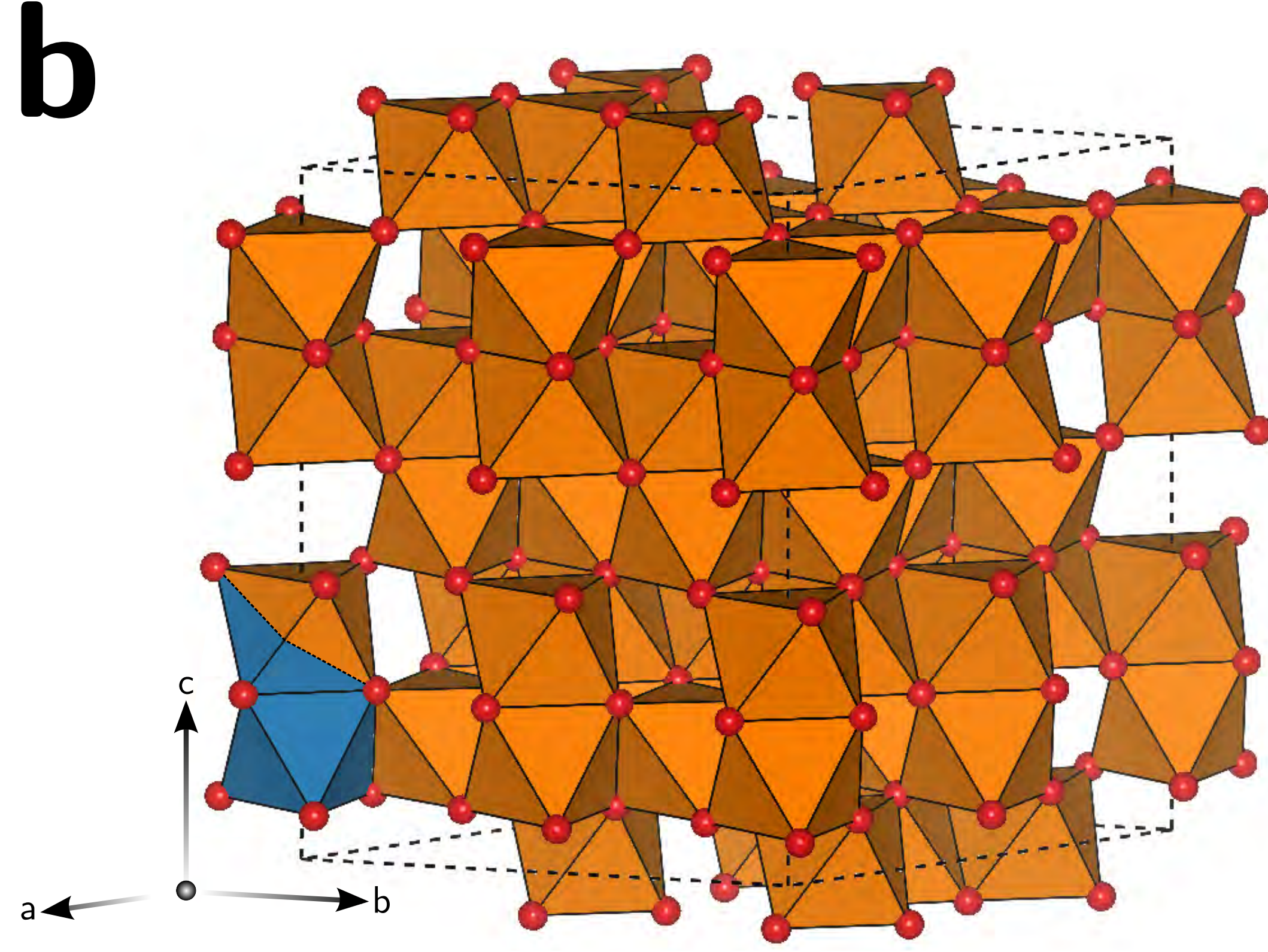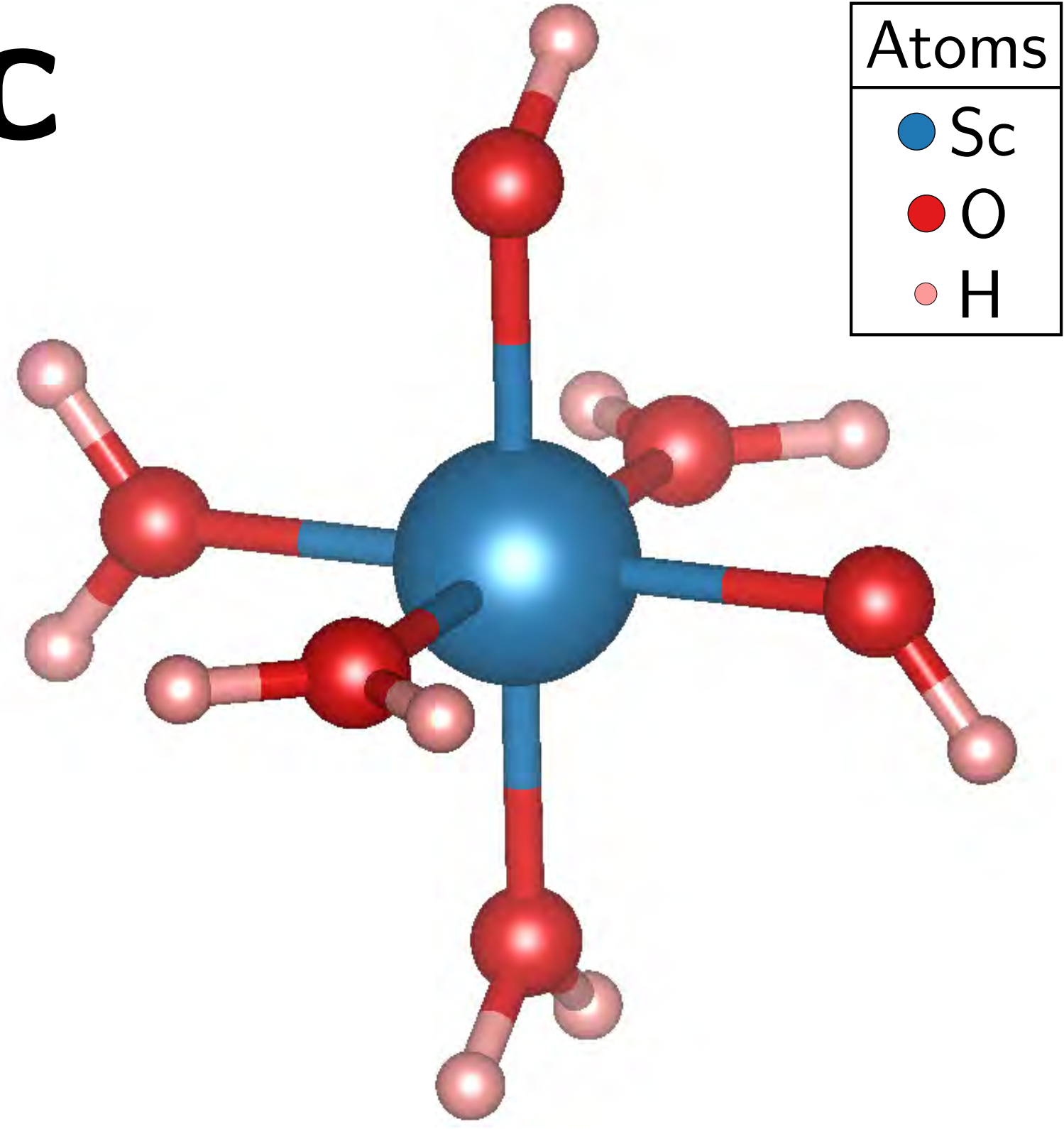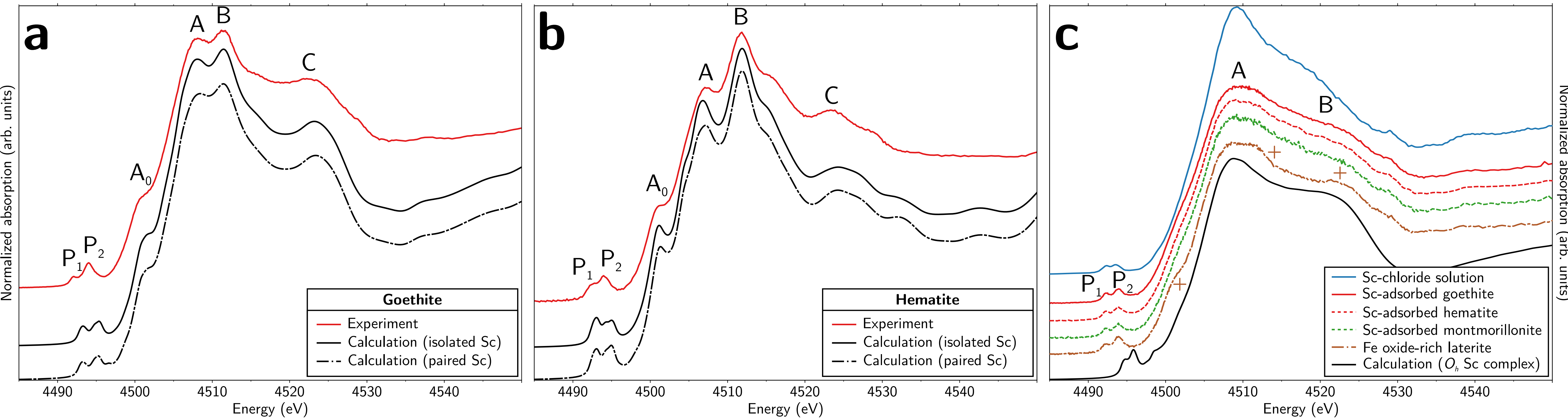|	Total energy (eV)	
Goethite	Sc-substituted goethite (isolated)	Sc-substituted goethite (paired)
39459.87	40037.77	40615.77
Hematite	Sc-substituted hematite (isolated)	Sc–substituted hematite (paired)
67718.57	68296.14	68873.69

Table S2

Figure 1

Figure 2

Figure 3